AGU FALL MEETING
New Orleans, LA & Online Everywhere
13–17 December 2021

[V25D-0155] Teleseismic moment tensor inversion for ring-faulting at active calderas: Case studies at Sierra Negra in the Galápagos Islands and Kilauea in Hawaii

Osamu Sandanbata[1], Hiroo Kanamori[2], Luis Rivera[3], Zhongwen Zhan[2], Shingo Watada[4], Kenji Satake[4], and Voon-Hui Lai[5]

(1) National Research Institute for Earth Science and Disaster Resilience, Japan, (2) California Institute of Technology, USA, (3) Université de Strasbourg, France, (4) The University of Tokyo, Japan, (5) Australian National University, Australia.

5-min. Summary Video is available in YouTube

Summary

- We suggest a method to estimate source parameters of ring-faulting at calderas using teleseismic data.
- Despite the instability of teleseismic moment tensor (MT) inversion for very shallow earthquakes, the resolvable MT components help us estimate some ring-fault parameters.
- By using the resolvable MT components of vertical-CLVD earthquakes at Sierra Negra and Kilauea, we could estimate ring-fault parameters that are consistent with those inferred from near-field observations.

1. Introduction

- **Ring-faulting** often occurs at calderas due to pressure change in a magma reservoir. Investigations of ring-faulting provide insights into volcanic processes.
- Ring-faulting can generate moderate-sized earthquakes of M_w>~5 characterized by moment tensors (MT) dominated by the vertical compensated-linear-vector-dipole (vertical-CLVD) component, called ***vertical-CLVD earthquakes*** (Ekström 1994; Shuler *et al.*, 2013; **Fig. 1**).

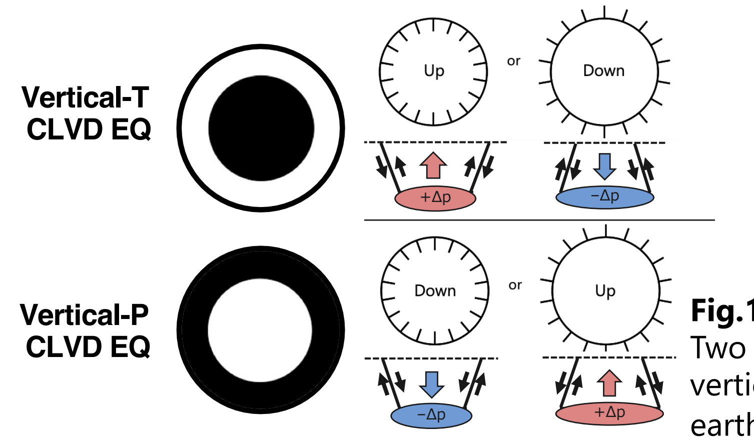

Fig.1 Two types of vertical-CLVD earthquakes.

"Is teleseismic MT inversion useful for ring-faulting study?"

2. Analysis

- The MT of the ring-faulting can be decomposed into three components: $\mathbf{M_{CLVD}}$ (vertical-CLVD), $\mathbf{M_{SS}}$ (vertical strike-slip), and $\mathbf{M_{DS}}$ (vertical dip-slip) (see **Figs. 2–3**) .

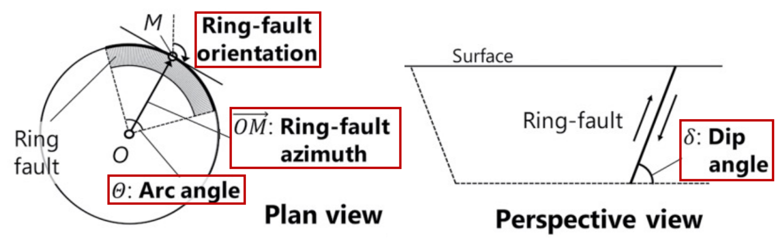

Fig. 2 Ring-fault parameters.

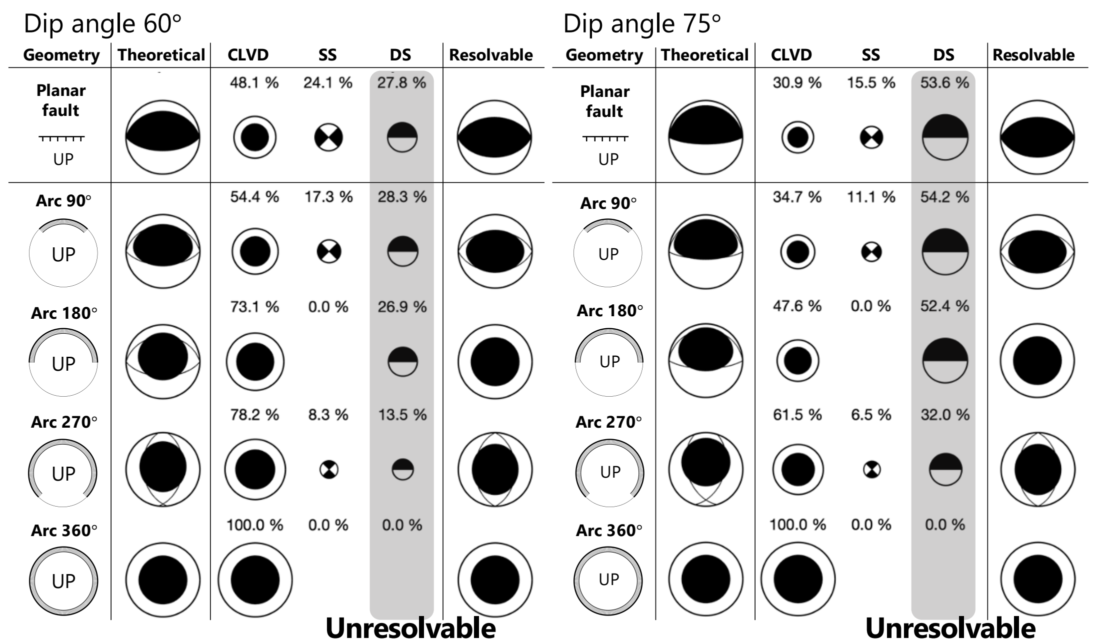

⬅Fig. 3 MTs and the components of ring-faulting with different *dip* and *arc angles*.

⬇Fig. 4 Synthetic long-period (80–200 s) waves from five elementary sources.

- Because ring-faulting usually occurs at a shallow depth <~5 km near the free-surface ($\tau_{r\theta} = \tau_{r\phi}$~0), $\mathbf{M_{DS}}$ ($M_{r\theta}$ & $M_{r\phi}$) excites only small long-period waves (**Fig. 4**); hence, $\mathbf{M_{DS}}$ ***is unresolvable from teleseismic data*** (Kanamori & Given, 1981).
- Here, we newly define *the* ***resolvable moment tensor***, excluding indeterminate $\mathbf{M_{DS}}$, as follows:

$$\mathbf{M_{res} = M_{CLVD} + M_{SS}}$$

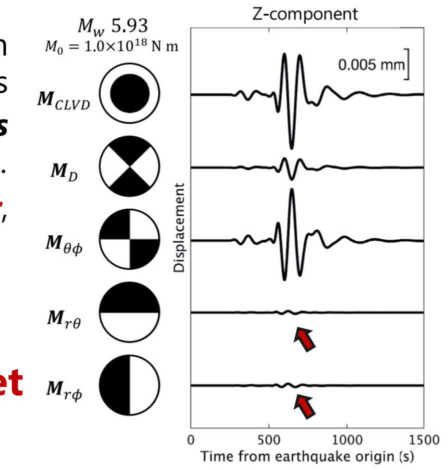

Due to the unresolvable $\mathbf{M_{DS}}$, we CANNOT interpret the MT directly; therefore, we use $\mathbf{M_{res}}$.

3. Methods for estimating *two* ring-fault parameters using M_{res}

1. Perform the deviatoric MT inversion using teleseismic data (period: >~50 s).
2. Obtain *the resolvable moment tensor* $\mathbf{M_{res}}$ by excluding $\mathbf{M_{DS}}$ (i.e., $M_{r\theta} = M_{r\phi} = 0$).
3. Estimate *the* ***ring-fault arc angle*** using *the CLVD ratio of* $\mathbf{M_{res}}$ (**Fig. 5a**):

$$k_{CLVD} = \frac{|M_{CLVD}|}{|M_{CLVD}| + |M_{SS}|} \times 100\ (\%)$$

4. Estimate *the* ***ring-fault orientation*** using *the Null(N)-axis direction of* $\mathbf{M_{res}}$ (**Fig. 5b**)
   - For arc angle < 180°: N-axis // Ring-fault
   - For arc angle > 180°: N-axis ⊥ Ring-fault

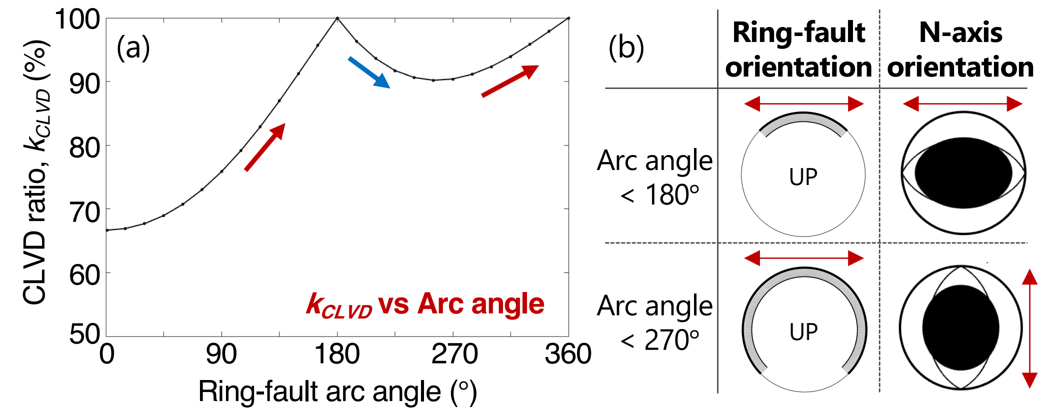

Fig. 5 Relationships (a) between k_{CLVD} *of* $\mathbf{M_{res}}$ & ring-fault arc angle, and (b) between the *N-axis orientation of* $\mathbf{M_{res}}$ and the *ring-fault orientation*.

By focusing on *the CLVD ratio & N-axis direction of* $\mathbf{M_{res}}$, we can constrain the *ring-fault orientation* and the *ring-fault arc angle*.

4. Stability test of M_{res} estimation

- We estimate $\mathbf{M_{res}}$ for a **vertical-T CLVD earthquake at Sierra Negra** on October 22, 2005, while shifting centroids around the caldera to examine its stability (depth is fixed at 2.5 km in the crust).
- As a result, **the estimation for $\mathbf{M_{res}}$ is very stable**, while the estimation for MT, including M_{DS}, is very unstable (**Fig.6**).

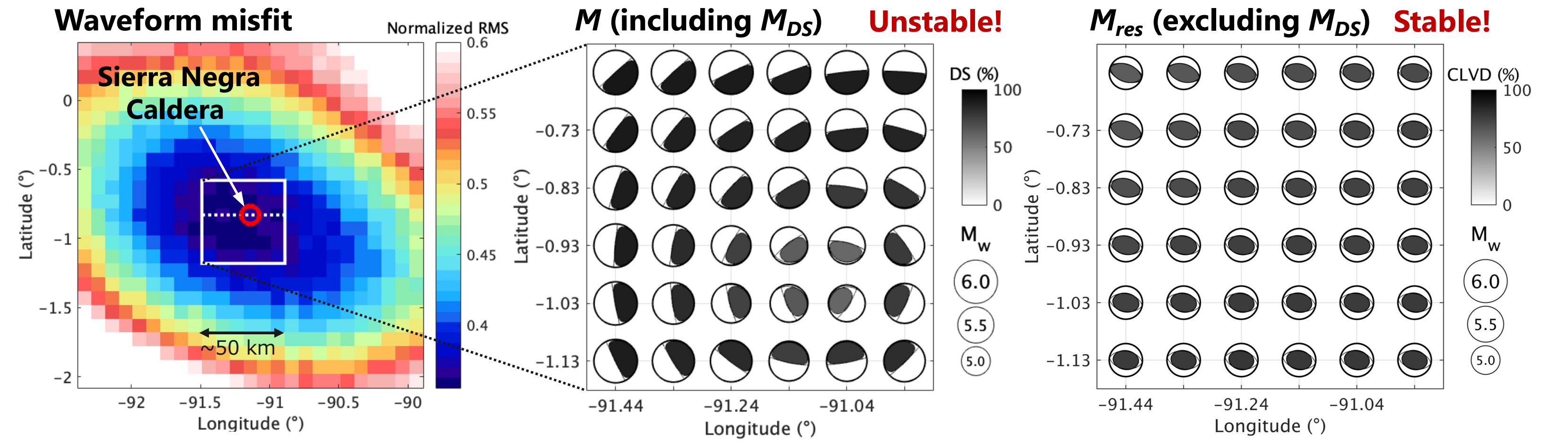

Fig. 6 (Left) Waveform misfits given by MT solutions at each centroid location. (Middle) MT solution ***M***, including $\mathbf{M_{DS}}$, and (Right) $\mathbf{M_{res}}$ at centroid locations around the caldera.

Despite the instability problem, $\mathbf{M_{res}}$ can be stably estimated with teleseismic data.

5. Results: Case studies

1. 2005 Vertical-T CLVD EQ at Sierra Negra (Galápagos)

- **Our estimation**: *Ring-fault orientation* = ~***NWW–SEE***, *Arc angle* = ~**80°**.
- **Field survey/geodetic analysis**: **Asymmetric ring-faulting** on the **southern-to-western side** of the caldera (Geist *et al.* 2008, Jónsson 2009).

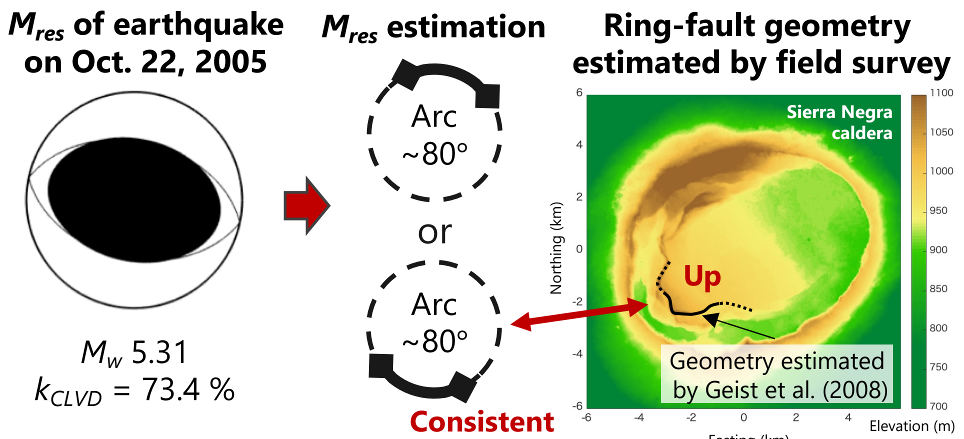

Fig. 7 (Left) $\mathbf{M_{res}}$. (Middle) Two candidates for ring-fault geometries estimated from $\mathbf{M_{res}}$. (Right) Geometry suggested in the previous studies,

Using $\mathbf{M_{res}}$, we could estimate ring-fault parameters that are consistent with those inferred from near-field observations.

2. Vertical-P CLVD EQs during the 2018 collapse at Kilauea (Hawaii)

- 50 earthquakes during the caldera collapse sequence showed similar $\mathbf{M_{res}}$.
- **Our estimation**: *Ring-fault orientation* = ~***NE–SW***, *Arc angle* <~**90°**.
- **Near-field seismic data**: **Asymmetric ring-faulting** on **NW or SE sides** of the summit caldera (Shelly & Thelen 2019, Lai *et al.* 2021).

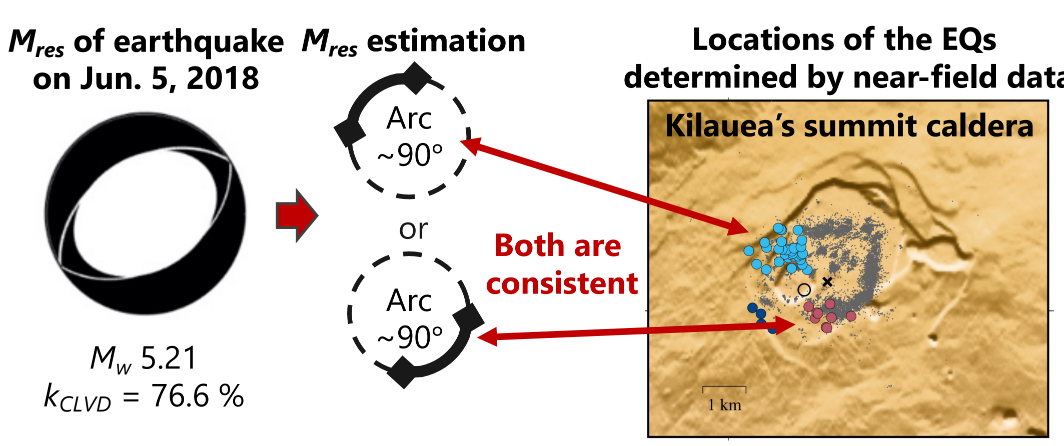

Fig. 8 (Left) $\mathbf{M_{res}}$. (Middle) Two candidates for ring-fault geometry estimated from $\mathbf{M_{res}}$. (Right) Earthquake locations determined by Shelly and Thelen (2019) (modified after figure from Lai *et al.* 2021). Circles and dots indicate locations of large vertical-P CLVD earthquakes and micro-seismicity, respectively.

6. Discussion

***Q1**. For estimating* $\mathbf{M_{res}}$ *, the isotropic component is assumed to be 0.* *How is* $\mathbf{M_{res}}$ *affected by* $\mathbf{M_{ISO}}$ *that may accompany ring-faulting?*

- Because of the waveform similarity between long-period waveforms from shallow $\mathbf{M_{ISO}}$ and $\mathbf{M_{CLVD}}$ sources (e.g., Kawakatsu 1996; **Fig. 9**), $\mathbf{k_{CLVD}}$ **may be biased** by a volume-change source with $\mathbf{M_{ISO}}$.

***Q2. What source parameters are lost** by removing* $\mathbf{M_{DS}}$ *?*

- The *ring-fault dip angle*, *azimuth*, and *slip amount* cannot be estimated solely with $\mathbf{M_{res}}$, since these parameters are controlled by $\mathbf{M_{DS}}$ (see **Fig. 3**).
- Since this method assumes pure dip slip, *oblique slip* may cause bias.

Note on Q2) The teleseismic-wave amplitude of shallow ring-faulting is in a trade off between *slip amount* and *dip angle*; hence, if we know either of the two from other observations, we may constrain the other using $\mathbf{M_{res}}$.

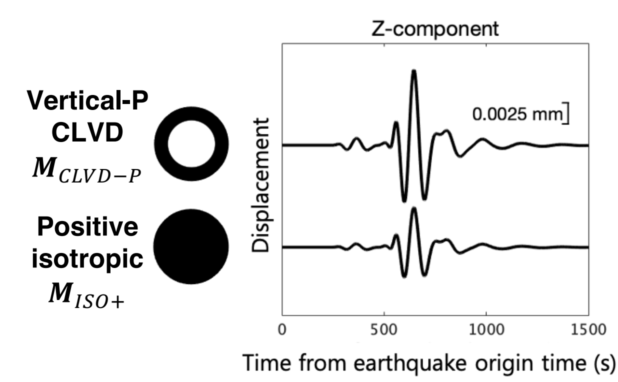

Fig. 9 Synthetic waveforms from the vertical-P CLVD source $\mathbf{M_{CLVD-P}}$, and the positive isotropic source $\mathbf{M_{ISO+}}$. Note that the waveforms are very similar.

Publications: You can find details of this work in two papers:

1. Sandanbata *et al.* (2021, JGR–Solid Earth)
2. Lai *et al.* (2021, JGR–Solid Earth).

See "REFERENCES" in iPoster Gallery for the paper information.

Acknowledgements: This study is funded by the JSPS KAKENHI (Grant numbers JP17J02919, JP20J01689, and JP19K04034), by the JST J-RAPID (Grant number JPMJJR1805), and partially by the Gordon and Betty Moore Foundation. We used broad-band seismic data downloaded from IRIS. For the inversion, we used the W-phase package (e.g., Kanamori & Rivera 2008).

S1. Efficiency of long-period teleseismic excitation from ring-faulting

- From computations of MTs for the ring-faulting, we show that the *steeper ring-faulting has a MT with larger M_{xz} and M_{yz} components*.

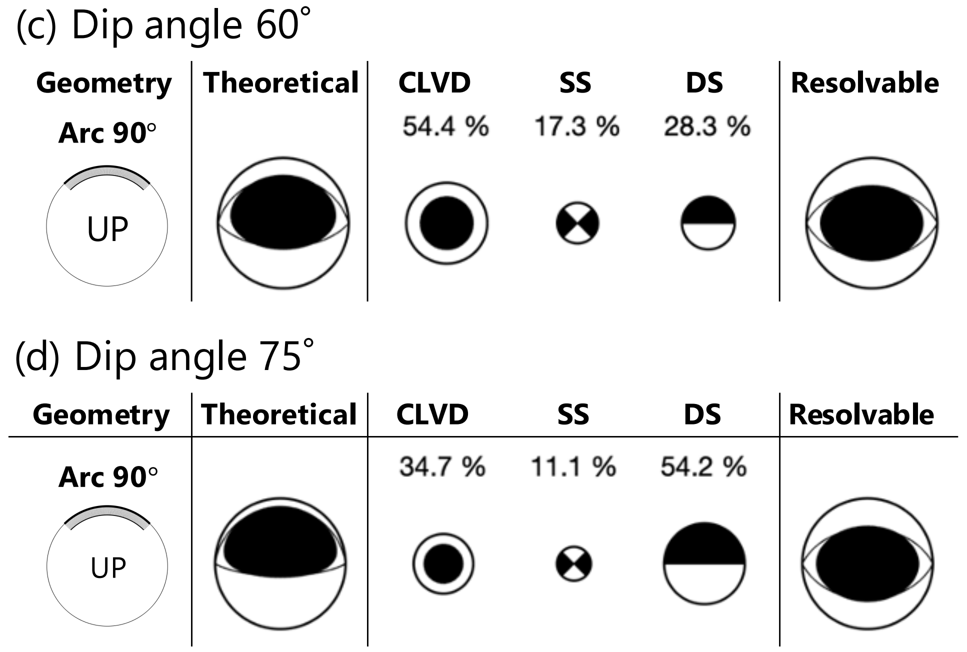

As the dip angle becomes **steeper** (more vertical), the ring-faulting contain **larger M_{xz}, and M_{yz}.**

Fig. S1 MTs and the components of ring-faulting with different *dip angles*.

- This means that the steeper ring-fault has components that do not contribute to radiations of the long-period teleseismic waves.

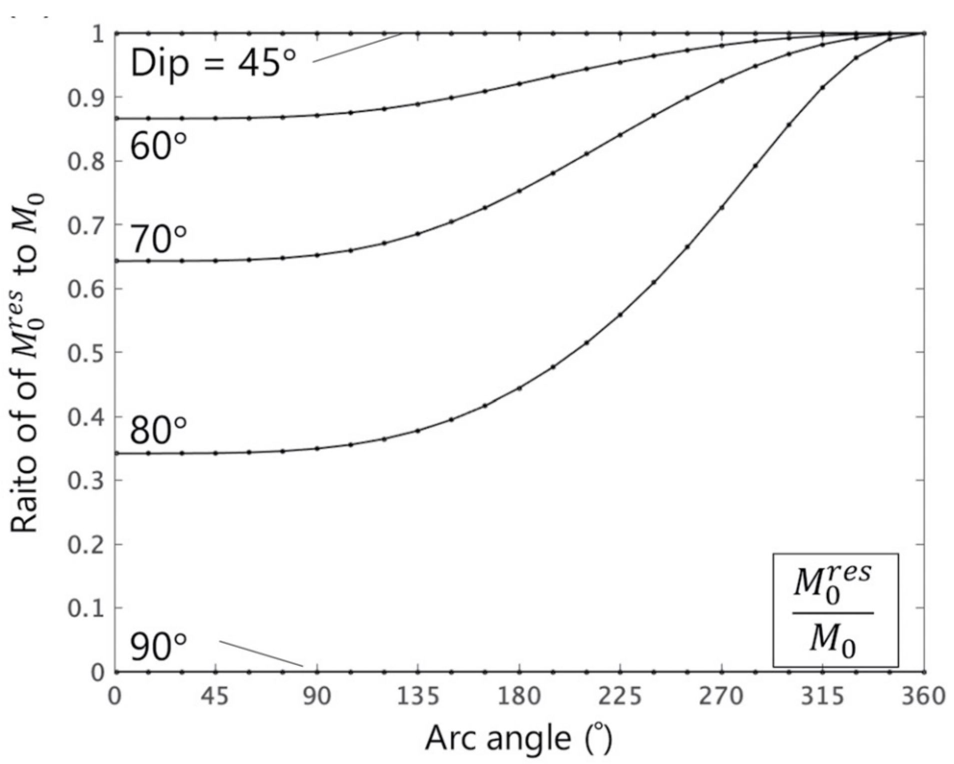

$$M_0^{res}/M_0$$

M_0: Seismic moment of ***M*** (including M_{xz} and M_{yz})

M_0^{res}: Seismic moment of $\boldsymbol{M_{res}}$ (excluding M_{xz} and M_{yz})

Fig. S2 The ratio of the seismic moment of ***M*** (M_0) to that of $\boldsymbol{M_{res}}$ (M_0^{res}), indicating the efficiency of the long-period teleseismic radiation.

Ring-faulting with steeper dip angle is less efficient in radiating long-period teleseismic waves.

S2. Case study 3: Two vertical CLVD EQs at Sierra Negra in 2018

- We also applied the method to two earthquakes in 2018 at Sierra Negra.

1. Vertical-T CLVD earthquake (M_w 5.3) on June 26, 2018 (~10h before the eruption)
2. Vertical-P CLVD earthquake (M_w 5.1) on July 5, 2018 (>a week after the eruption)

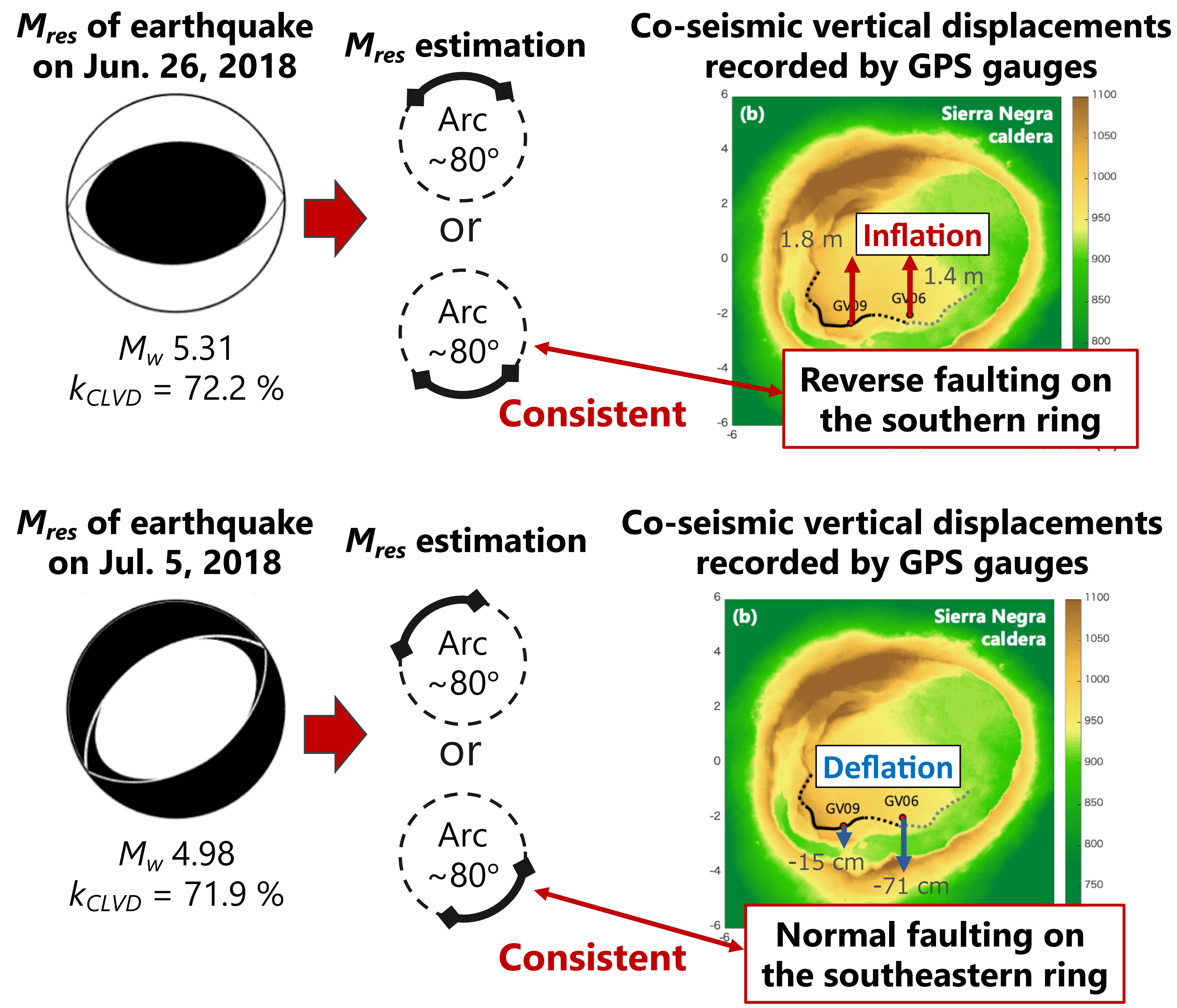

Fig. S3 Applications to two vertical-CLVD earthquakes on (top) June 26, and (bottom) July 5. In each, (Left) $\boldsymbol{M_{res}}$. (Middle) Two candidates for ring-fault geometries estimated from $\boldsymbol{M_{res}}$. (Right) Co-seismic displacements recorded by GPS data, following Bell et al. (2021).

The differences between M_{res} for the two vertical-CLVD EQs indicates the changes in source locations along the fault system, as well as in the source kinematics.

Schematic shows the chronology of the Kīlauea summit deformation during the 2018 Kīlauea eruption (Lai *et al.* 2021)

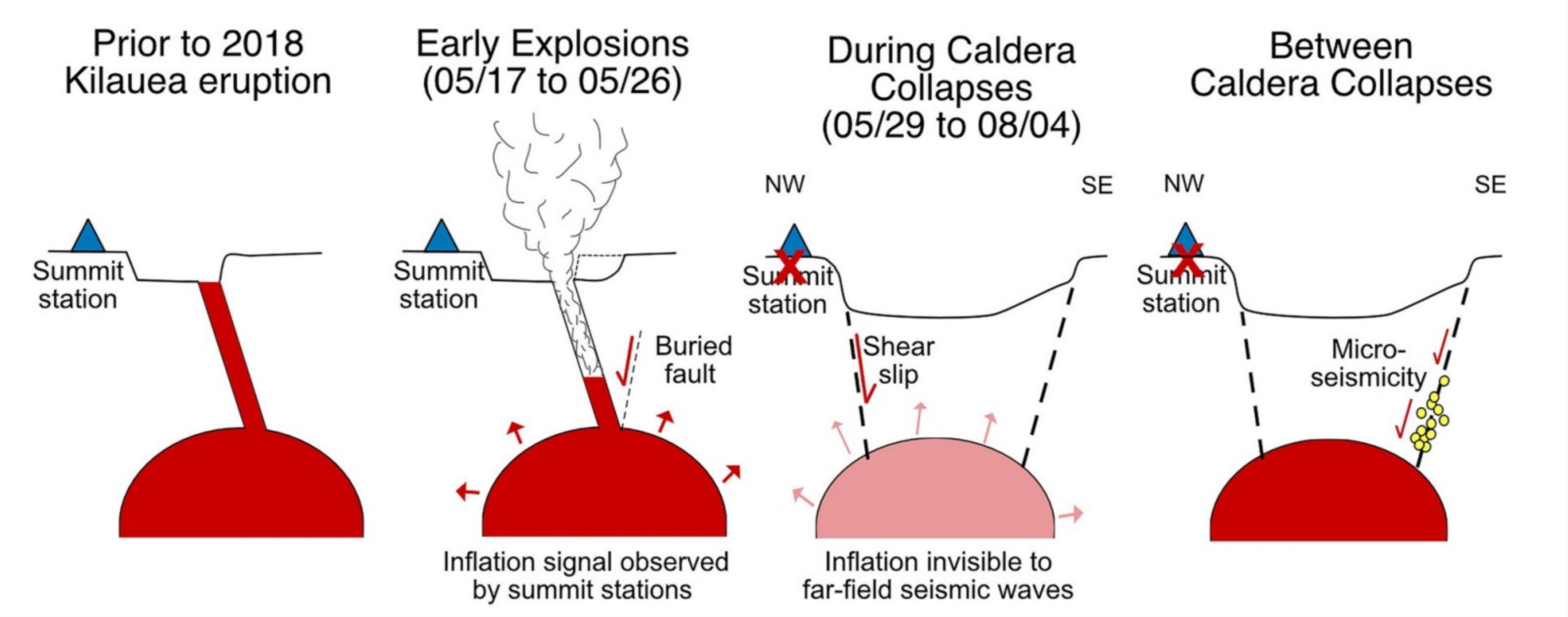

Cartoon cross-sections depicting the inflation-deflation cycle of the 2018 eruption and plumbing system at Sierra Negra (Bell *et al.* 2021)